

# Annual Cycle of Hygroscopic Properties and Mixing State of the Suburban Aerosol in Athens, Greece.

Christina Spiteri<sup>1</sup>, Maria Gini<sup>1</sup>, Martin Gysel-Beer<sup>2</sup> and Konstantinos Eleftheriadis<sup>1</sup>

<sup>1</sup> Environmental Radioactivity Laboratory, Institute of Nuclear and Radiological Science & Technology, Energy & Safety, NCSR Demokritos, 15310 Ag. Paraskevi, Athens, Greece

<sup>2</sup> Laboratory of Atmospheric Chemistry, Paul Scherrer Institute, Forschungsstrasse 111, Villigen PSI, Switzerland

*Correspondence to:* Christina Spiteri (spiteri@ipta.demokritos.gr) and Maria Gini ([gini@ipta.demokritos.gr](mailto:gini@ipta.demokritos.gr))

**Abstract.** The hygroscopic properties of atmospheric aerosol were investigated at a suburban environment in Athens, Greece, from August 2016 to July 2017. The Growth Factor Distribution Probability Density Function, (GF-PDF), and mixing state were determined with a Hygroscopicity Tandem Differential Mobility Analyzer, (HTDMA). Four dry particle sizes, ( $D_0$ ), were selected to be analyzed in terms of their hygroscopic properties at 90 % relative humidity. The annual mean GFs for  $D_0 = 30$ , 50, 80, and 250 nm, were found to be equal to 1.28, 1.11, 1.13, and 1.22, respectively. The hygroscopic growth spectra were divided into two distinct hygroscopic ranges; a non and/or slightly hygroscopic mode ( $GF < 1.12$ ) and a moderately hygroscopic mode ( $GF > 1.12$ ), which are representative of a suburban environment influenced by local/urban emissions and background aerosol. The standard deviation  $\sigma$  of the GF-PDF was employed as a measure of the mixing state of ambient aerosol. The 30 nm particles were mostly internally mixed, whereas larger particles were found to be externally mixed, with either a distinct bimodal structure or with partly overlapping modes. Cluster analysis on the hourly dry number size distributions, was performed to identify the link between aerosol hygroscopicity and aerosol emission sources and formation processes. The size distributions were classified into five groups, with the “mixed; urban and regional background” aerosol (67%) and the “fresh traffic-related particlesurban nocturnal” from the neighbourhood urban area (15 %) aerosol (12%) to account for more than 80 79% of the results. The hygroscopic properties for 50 nm and 80 nm were found to be similar in all cases, indicating particles of similar nature and origin across these sizes. This was also confirmed through the modal analysis of the average number size distributions for each cluster; the 50 nm and 80 nm particles were found to belong to the same Aitken mode in most cases. The 250 nm particles (i.e. accumulation mode) were generally more hygroscopic than Aitken particles, but less hygroscopic than the 30 nm particles (nuclei mode).

## Introduction

Atmospheric aerosol particles in the ambient atmosphere affect the radiation budget of the planet and the regional and global climate (IPCC, 2013; Rosenfeld et al., 2014), through direct and indirect effects (Li et al., 2016). Aerosol particles interact

with solar radiation through light absorption and scattering, inducing a positive or negative radiation forcing, respectively (Haywood and Boucher, 2000). Additionally, aerosol particles can act either as cloud condensation nuclei (CCN) or as ice nuclei (IN), which determines their indirect effect on cloud's microstructure and lifetime. The climate-relevant properties of atmospheric aerosol particles are largely influenced by their ability to take up water, (hygroscopicity), and their state of mixing-  
35 (Zhang et al., 2011; Kaufman et al., 2002; McFiggans et al., 2006).

The hygroscopic properties of atmospheric particles are strongly related to particle chemical composition (Gunthe et al., 2009; Gysel et al., 2007), while they undergo continuous changes over particle lifetime. Research results have shown that the relative non-hygroscopic fresh organic aerosol can become hygroscopic through physical and chemical atmospheric processes (Kanakidou et al., 2005). This is also the case for soot particles originating from different sources (e.g. biomass burning, diesel  
40 soot). Condensation of secondary species on the surface of primarily emitted soot, (pure black carbon particles), may alter their hygroscopic properties from non-hygroscopic, to hygroscopic being therefore capable to act as CCN (Tritscher et al., 2011; Kotchenruther and Hobbs, 1998). Motos et al., (2019) also studied and established the relations between the black carbon core size, mixing state and droplet activation.

Aerosol hygroscopic growth can be measured or estimated by both direct and indirect techniques (Dean A. Hegg et al., 2007,  
45 P. Achtert et al., 2009). The most widespread real-time direct measurement technique for fine mode aerosol is the Hygroscopicity Tandem Differential Mobility Analyzer, (HTDMA), which determines the Growth Factor, (GF), of particles at a given dry particle diameter and relative humidity, (RH). Then, the hygroscopic parameter  $\kappa$ , a simplified parameter model the composition-dependence of the solution water activity can be calculated as described by Peter and Kreidenweis (2007). The kappa values for highly hygroscopic aerosols, such as salts and sulfates, range between 0.5 and 1.4, for organics from  
50 0.01 to 0.5, whereas for non – hygroscopic aerosol such as soot, the kappa values are close to zero (Bezantakos et al., 2013; Gysel et al., 2007).

The cloud nucleating effectivity of aerosol particles and the overall aerosol-cloud-climate interactions, depend on the distribution of components among individual particles, termed as "aerosol mixing state" (Riemer et al., 2019). Ambient aerosol is usually considered a heterogeneous mixture of particles with different chemical compositions and sizes. We refer  
55 to an internal mixture of aerosol when the particles of the same size have similar chemical composition. Whereas, in an external mixture particles of the same size have distinctly different chemical composition. The aerosol in urban/sub-urban environments typically is an external mixture of non-hygroscopic aerosol from fresh local emissions and moderately hygroscopic background aerosol (Wang et al., 2018; Enroth et al., 2018; Swietlicki et al., 2008), whereas in marine environments the aerosols tend to be internally mixed and highly hygroscopic (Massling et al., 2007).

60 Long-term measurements of aerosol hygroscopicity are commonly done using CCN counters (e.g. Paramanov et al., 2015, Schmale et al. 2017, Schmale et al., 2018 and references therein) or HTDMAs. A few long-term studies of aerosol hygroscopicity and mixing state by means of the HTDMA technique have been published so far, and some of them are mentioned below (Kammermann et al., 2010, Fors et al., 2011, Holmgren et al. 2014). These provide a better understanding of the link between particle hygroscopic growth and particle emission sources, formation and transformation processes. The

65 present study aims at providing insights into the hygroscopic properties and state of mixing of ambient aerosol and the origin of ambient ultrafine and fine particles, through 1 year of measurements of key microphysical parameters (i.e. size distributions and time- and size- resolved HTDMA data) in a suburban environment. The hygroscopicity of ambient aerosol was investigated in the particle size range between 30 [nm](#) and 250 nm, providing information about the month-to-month variability, seasonal cycle and diurnal pattern of hygroscopicity and the degree of mixing state for selected particle sizes.

70

## 2. Methodology

### 2.1 Sampling Site

75 The measurement campaign was conducted from August 2016 to July 2017, at the Demokritos (DEM) station (fig.1.), member of GAW and part of the ACTRIS and PANACEA infrastructures within the National Centre of Scientific Research Demokritos campus. The station is located in a vegetated area at the foot of Mount Hymettus, about 7 km to the North east from Athens city centre. It is an urban background station, representative of the atmospheric aerosol in the suburbs of the Athens Metropolitan Area. The site is partially influenced by transported pollution from the urban area of Athens (Eleftheriadis et al., 2021) (i.e. under most atmospheric conditions) and partially by the incoming regional aerosol (i.e. under Northern, Southern 80 or Eastern winds).



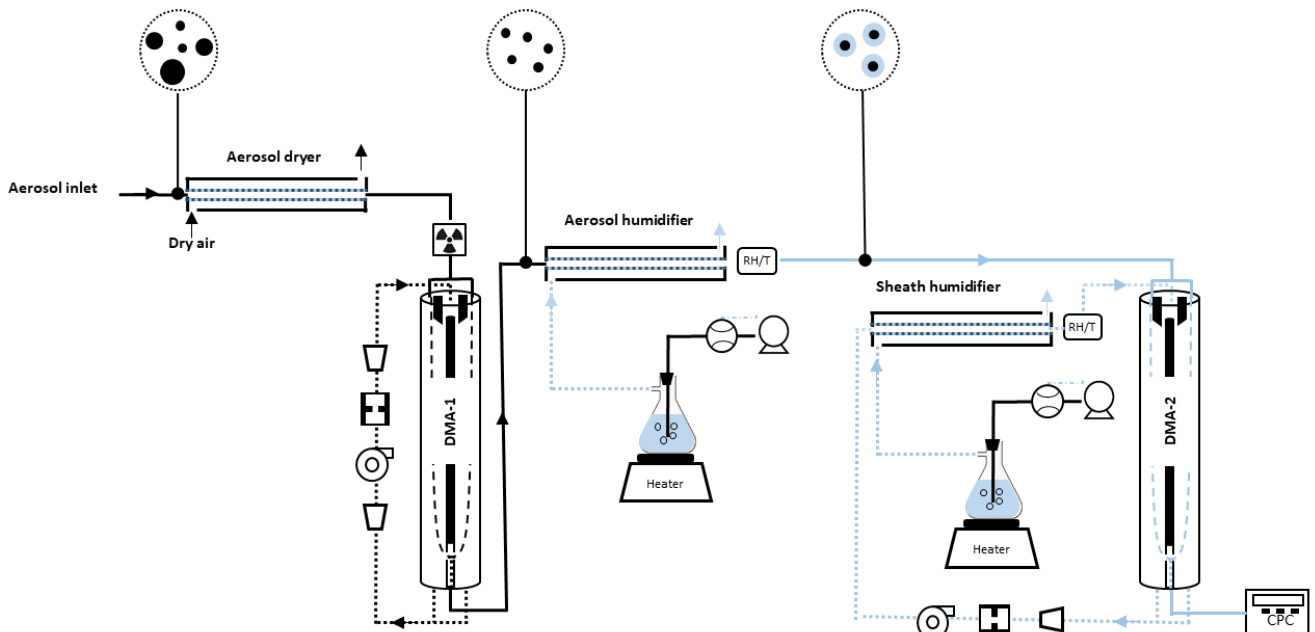
**Figure 1** The Demokritos Atmospheric Aerosol Measurement station in Athens, (from © Google Maps).

### 2.2 Instrumentation

85

A custom-built Humidified Tandem Differential Mobility Analyzer, (HTDMA), was used to measure the hygroscopic growth factor distributions of ambient aerosol particles with selected dry diameters,  $D_{0,\text{--}}$  at certain narrow size fractions centered

around 30 nm, 50 nm, 80 nm and 250 nm and exposed at relative humidity (RH) of  $90 \pm 2 \%$ , (Bezantakos et al., 2013). Figure 2 shows the main components of the HTDMA system. The HTDMA consists of two differential mobility analyzers (DMAs) in tandem mode, a humidifier section and a condensation particle counter (CPC 3772, TSI). The polydisperse aerosol was initially dried, passing through an aerosol Nafion dryer, and brought to charge equilibrium passing through a  $^{85}\text{Kr}$  bipolar neutralizer, before entering the first DMA, (DMA-1), where the specific particle sizes were selected (monodisperse aerosol), according to their electrical mobility. Then, the monodispersed and dried particles were conditioned, by passing through the humidifier section, at a well-defined relative humidity (set point 90 %), before entering the second DMA (DMA-2); the sheath flow of the DMA-2 was also humidified at a relative humidity of 90 %. The DMA-2 was operated with the CPC in a scanning mobility sizer configuration (SMPS), to measure the particle size distribution of the conditioned wet aerosol. Both DMAs were operated with a sheath flow rate of 3 L/min, and a sample flow rate of  $\sim 0.3$  L/min.



100

**Figure 2** Schematic diagram of the HTDMA system

The aerosol number size distributions of ambient aerosol (dry), were measured by means of a Scanning Mobility Particle Sizer system (SMPS), operated in parallel with the HTDMA at the DEM station. The SMPS consists of an electrostatic classifier (TSI Inc. model 3080), a cylindrical differential mobility analyzer column (TSI Inc, model 3081), and a condensation particle counter (TSI Inc., model 3772). It was operated with a five-minute time resolution and an aerosol-to-sheath flow ratio of 1/5 lpm covering a particle size range from 10 nm to 550 nm. Both aerosol and sheath flows were dried to relative humidity lower

than 40% using a Nafion drier. Data acquisition and analysis was performed using the TROPOS-SMPS data evaluation software, (Wiedensohler et al., 2012). To achieve the highest measurement accuracy with SMPS measurements, the technical recommendations and quality control procedures proposed by Wiedensohler et al. (2012) were followed.

The standard meteorological parameters (i.e. temperature, humidity, wind speed and wind direction) were recorded at an hourly time interval at DEM station. The meteorological sensors were installed on a meteorological mast, at 10 m height above ground.

## 2.3 Data analysis

### 115 2.3.1 HTDMA data inversion and fitting procedure

Due to water uptake, the diameter of the humidified particles ( $D(RH)$ ) increase, and the ratio between humidified<sub>7</sub> ( $D(RH)$ ), and dry particle diameter<sub>5</sub>  $D_0$ , is defined as the Growth Factor (GF):

120 
$$GF = \frac{D(RH)}{D_0}, \quad (1)$$

where<sub>5</sub>  $D(RH)$  is the particle diameter at the given RH and  $D_0$  is the dry diameter selected by the first DMA. The particle concentration at the HTDMA outlet as a function of Growth Factor<sub>7</sub> (GF), set at the HTDMA is referred to as Measurement Distribution Function<sub>5</sub> (MDF).

125 Then, an inversion algorithm was applied to the measured MDF to retrieve the actual Growth Factor Probability Density Function (GF-PDF), which describe the probability that a particle with a defined dry size exhibits a certain GF at the specified relative humidity. The methodology we follow for inverting the HTDMA data is described in detail by Gysel et al. (2009). A key element for the data inversion is the Kernel function, which describes the physics of a TDMA system. The Kernel width calibration, for particles exhibiting a true growth factor of 1.0, of the HTDMA and data inversion, were performed according  
130 to the methodology described by Gysel et al. (2009), applying the TDMAinv algorithm. The underlying principle of the HTDMA inversion approach is to find an inverted GF-PDF, such that a minimum  $\chi^2$  -residual is obtained between the measured MDF and the reconstituted MDF<sub>5</sub> (R-MDF). The Growth Factor Probability Density Functions (GF-PDFs) were afterwards normalized to unity. The GF-PDFs measured in the range  $88 \% < RH < 92 \%$  were recalculated to  $RH = 90 \%$  following the procedure described by Gysel et al. (2009), in order to minimize uncertainties associated with variations in RH levels. Each  
135 GF-PDF was described as a piecewise linear function with the midpoint of the first and last inversion bin at  $GF=0.7$  and  $GF=2.5$ , respectively, and a resolution of  $\Delta GF=0.1$ . The GF standard deviation<sub>5</sub>  $\sigma$ , of a GF-PDF, was also determined according to Eq. (C.6) in Gysel et al. (2009).

The  $\sigma$  is used as a measure for the spread of growth factor to describe the mixing state (Sjogren et al., 2008).

In the present study, the inverted data were grouped into three cases, representative of the aerosol mixing state in fig. 3.  
140 Specifically,  $\sigma \leq 0.07$  indicates an internally mixed aerosol (fig.3, Panel A),  $\sigma \geq 0.15$  describes an externally mixed aerosol

with two distinct modes (fig.3, Panel C), whereas GF-PDFs with  $0.07 < \sigma < 0.15$  are considered as a continuum of mixing states with two overlapping modes or a broad mode (fig.3, Panel B), (almost bimodal and externally mixed). The bimodal GF-PDFs spectra, either with overlapping or with well-defined modes, ~~was-were~~ divided into two distinct ranges of particle hygroscopicity: one subset comprising non and/or slightly hygroscopic particles with  $GF < 1.12$ , the other subset comprising moderately hygroscopic particles with  $GF > 1.12$ . This threshold GF coincides with the typical local minimum in the GF-PDFs observed in this study, which also is in line with the findings of previous studies (Kim et al., 2020). Then the different integral properties of GF-PDFs (i.e. mean GF and number fraction), for these subranges, were calculated by Eq. (C.9) and Eq. (C.8), as described by Gysel et al., (2009), by averaging GF-PDFs above and below the  $GF = 1.12$  threshold. It has been noted that a sensitivity analysis has been performed before selecting the two subranges, by changing the selected threshold GF between 1.12 and 1.20 with no significant effect on the calculated parameters. The fixed GF threshold translates to slight size dependence of the kappa threshold, i.e. from 0.07 to 0.05 for 30 nm to 250 nm.

150 Additionally, the hygroscopicity parameter  $\kappa$ , was calculated as follows (Petters and Kreidenweis, 2007):

$$\kappa = \frac{(GF^3 - 1)(1 - a_w)}{a_w} \quad (2)$$

155

156 Where  $a_w$  is the water activity, at which the growth factor was measured. According to Köhler theory (Köhler, 1936),  $a_w$  is obtained by

$$a_w = \frac{RH}{\exp\left(\frac{4\sigma_s v_w}{RTD}\right)} \quad (3)$$

160

161 where  $\sigma_s$  is the surface tension of the solution droplet (assumed to be pure water),  $v_w$  is the partial molar volume of water in solution,  $R$  is the universal gas constant,  $T$  is the temperature, and  $D$  is the diameter of the droplet.

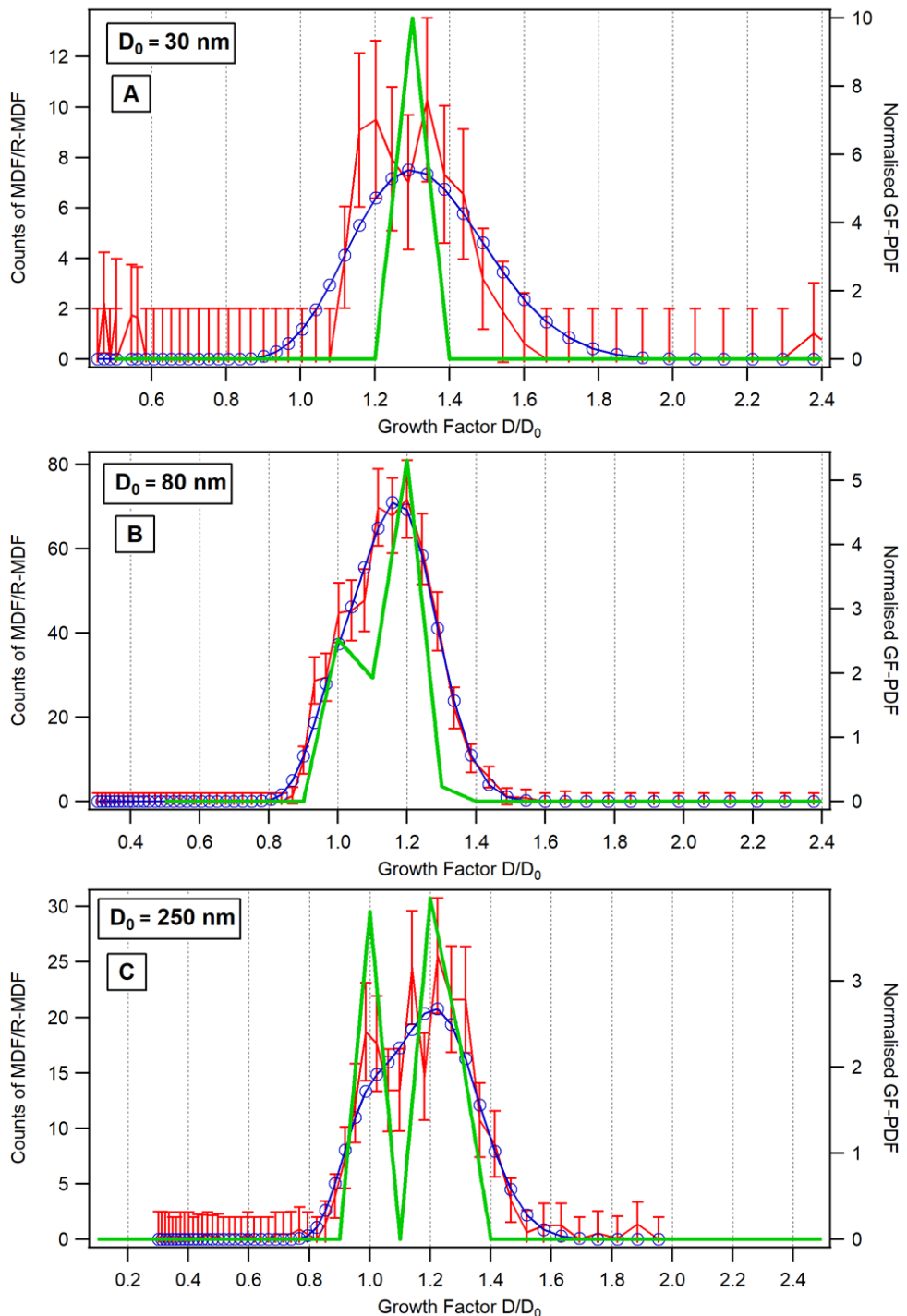


**Figure 3** Example of growth factor distributions measured at RH=90% of  $D_0=30\text{nm}$  particles (Panel (A), internally mixed), of  $D_0=80\text{nm}$

165 particles (Panel (B), continuum of mixing states) and of  $D_0=250\text{nm}$  particles (Panel (C), externally mixed with distinct modes). The line

represents the measured particle counts, the blue line represents the reconstructed measured distribution function and the green line is the GF-PDF.

One of the limitations of the HTDMA technique for size resolved hygroscopicity measurements arises from selecting several representative size fractions to study but at the same time obtaining data in a relatively high time resolution. In our case, four dry sizes were selected to be studied i.e. 30 nm, 50 nm, 80 nm and 250 nm. Our findings reveal that the 50 nm and 80 nm Aitken particles presented similar hygroscopic properties, whereas larger differences were observed between the Aitken particles and the particles in the accumulation size range i.e. 250 nm. At least from a CCN-prediction perspective, our size selection might not be the optimal one, although the GF-PDFs can be interpolated in time and diameter in between the available measurements to describe the hygroscopic behaviour of the aerosol particles in each size bin of the SMPS, without introducing too much error in CCN predictions as confirmed by previous studies (Kammermann et al., 2010). Alternatively, it might be more ideal the hygroscopic properties of ambient aerosol at the dry diameter,  $D_0$ , 60 nm and 120 nm, instead of at 50 nm and 80 nm, to be investigated given that the size range between 100 and 150 nm is considered very important for CCN studies.

### 180 **2.3.2 Cluster Analysis**

k-means cluster analysis was applied to the hourly-average particle number size distributions to classify the distributions of the highest degree of similarity into the same cluster, reducing in that way the complexity of the dataset. The k-means method aims to minimize the sum of the squared Euclidian distance between each dataset point and the corresponding cluster center (i.e. the mean of all the points in a cluster). Cluster analysis was performed using the IBM SPSS software. The interpretation of the origin of each cluster was based on the dominant size modes (Hussein et al., 2014), their hourly frequency of occurrence and the average values obtained for standard meteorological parameters.

### 190 **2.3.3 Multimodal Analysis**

The modal characteristics of the clustered average number size distributions were obtained by applying a curve-fitting algorithm as proposed by Hussein et al. (2005). The least squares method was used to best-fit the sum of up to 4 modes to the multi-modal distributions to the clustered number size distributions. The log-normal distributions were described by the following characteristic modal parameters of each mode: geometrical mean mobility diameter, number concentration and geometric standard deviation. Starting from an initial assumption, the modal parameters of each log-normal distribution were successively re-defined to obtain the best-fit curve. The algorithm starts by fitting a uni-modal log-normal distribution, and successively tests the possibility of increasing it to a bi-, a tri- and finally a tetra-modal distribution. The optimum best-fit curve was determined by minimizing the root mean square error (RMSE, %), defined as Vratolis et al. (2019),

200  $RMSE = \frac{100}{\sqrt{n}} (\sum_{i=1}^n (N_{dpi}^m - N_{dpi}^f)^2)^{0.5}$  (4)

where n is the number of size bins of the SMPS size distribution,  $N_{dpi}^m$  is the number concentration measured by the SMPS at size bin i corresponding to particle diameter dpi, and  $N_{dpi}^f$  is the number concentration of the sum of fitted modes at diameter dpi.

205

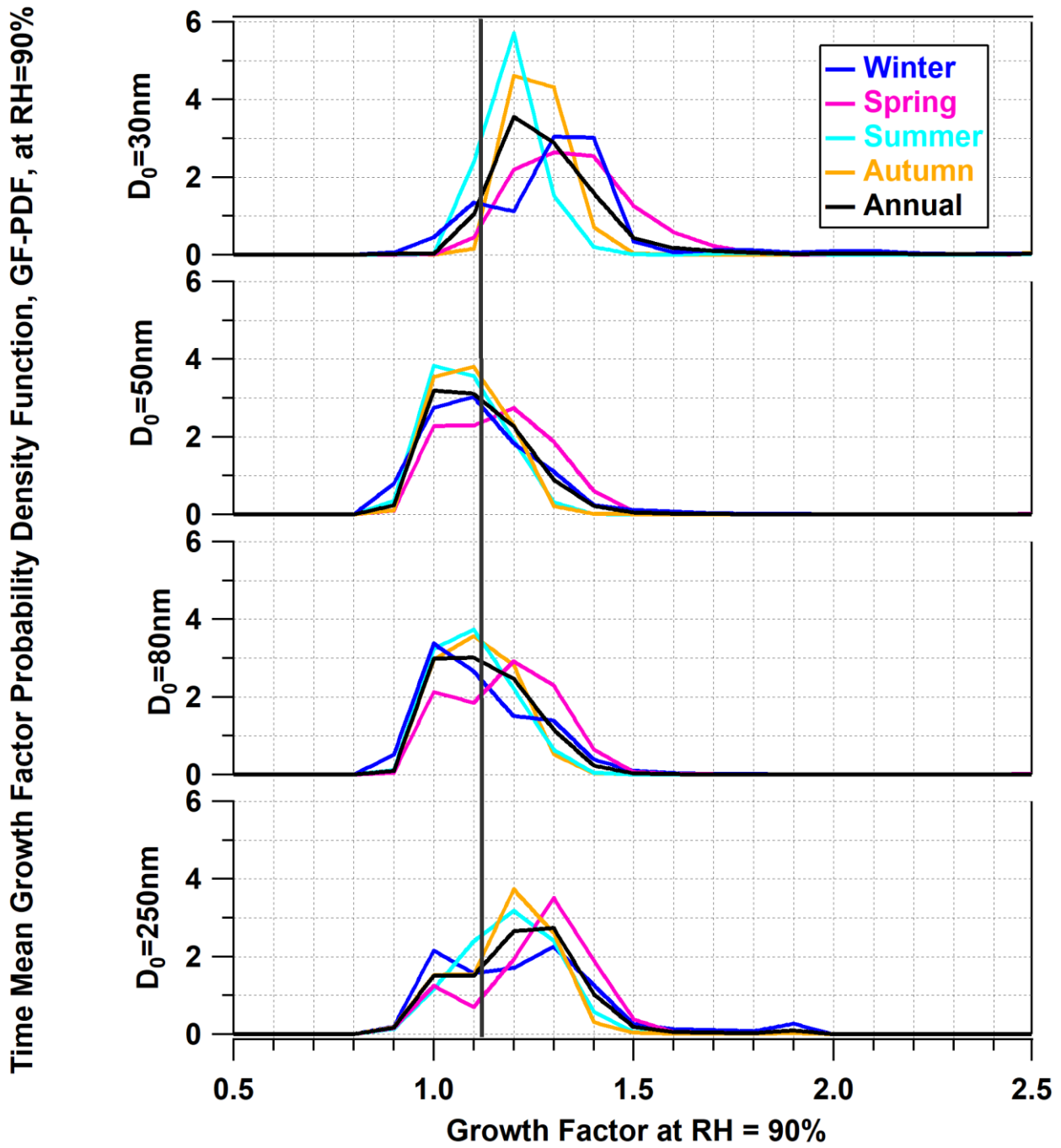
### 3. Results and Discussion

#### 3.1 Seasonal and monthly variability of aerosol GF and mixing state

210 The seasonal, as well as the annual, mean GF-PDFs, fig. 4., were calculated by averaging the individual GF-PDF for each dry particle size and season. The GF-PDFs represent the mean distributions of the growth factors of particles with  $D_0 = 30, 50, 80$  and  $250 \text{ nm}$ . The selected dry sizes are representative of the nuclei (30nm), Aitken (50 and 80nm) and accumulation (250nm) mode of the aerosol number size distributions, respectively. It has to be highlighted that the mean GF-PDFs represent the mean distributions of growth factors and does not necessarily provide a clear picture of the mixing state of these size fractions. In specific, the appearance of a broad mode or two overlapping modes or two distinct modes does not imply the simultaneous<sup>ly</sup> 215 existence of particles with distinctly different hygroscopic properties and therefore compositions, but it may also result as a matter of GF temporal variability. Below it will be further discussed and clarified which factor is the prominent one at different cases. The majority of the mean GF-PDFs of the nuclei mode particles with dry diameters of 30 nm were characterized by a unimodal peak, during all seasons, except from winter, with GFs to be ranging between 1.17 and 1.41, as reported in Table S1. Non and/or slightly hygroscopic 30-nm-particles with GF~1.0 are essentially missing, in contrast to particles with  $D_0 > 220 30 \text{ nm}$ , indicating that bare black carbon particles do not make a dominant contribution at this size either because sources of other particle types are stronger or because they rapidly acquire some hygroscopic coatings.

In winter time, is observed a complex state of mixing was observed indicating that both (two modes) the existence of two modes fresh (non and/or slightly hygroscopic) and aged (more hygroscopic) combustion-generated nanoparticles (i.e. biomass burning, traffic) contribute to the nuclei mode, with the time scale and efficiency of the aging process governing the final 225 hygroscopic properties and state of mixing (Wang et al., 2018; Enroth et al., 2018; Swietlicki et al., 2008, Kim et al., 2020, Vu et al., 2021). indicating that probably both fresh, (non and/or slightly hygroscopic), and aged, (moderately hygroscopic), emissions from traffic and other combustion sources, (biomass burning, residential heating), produce particles of different chemical composition with the time scale of aging governing their hygroscopicity (This conclusion is supported by the studies we refer to for Athens and other urban areas (Wang et al., 2018; Enroth et al., 2018; Swietlicki et al., 2008,) as well as recent 230 studies (Kim et al., 2020) contribute to the 30 nm size fraction. The relative contribution from different emissions sources in each mode could not be determined due to the temporal variability of the spread factor  $\sigma$  and the growth factor of particles, which means that both regional background and local sources are likely contributors.

235 In general, the externally mixed nature of the nuclei mode reflects the less efficient aging and coating of the fresh combustion-related nanoparticles during the dark and cold months of the year. The aging processes are more efficient for the nuclei mode rather than the higher Aitken modes in modifying their hygroscopicity due to condensation of oxidised species, oxidised species, organics and inorganics of coating effect of sulfates and secondary organics and due to condensation of water soluble material onto the pre-existing nuclei particles, which are more significant for smaller particles (Petäjä et al., 2007, Vu et al., 2021, Tritscher et al., 2011, Guo et al., 2016). The fact that 30 nm aerosol particles are characterized as externally mixed only during wintertime is a combined effect of the time scale of the aging process, which is not very effective during the dark and colder months, and the relative contributions of fresh and background aerosol at the background location of the DEM station. More detailed discussion for this fraction will follow further below.



245 **Figure 4** Seasonal and annual mean GF-PDFs for different dry particle sizes (30, 50, 80 and 250 nm). The vertical black line represents the  
selected cut-off between the non and/or slightly hygroscopic mode (GF<1.12) and the moderately hygroscopic mode (GF>1.12).

The GF-PDFs of medium to large Aitken mode particles, i.e. at 50 nm and 80 nm, characterized by a broad peak, within the range of 1.00 and 1.27, (Table S1). The contribution of the non and/or slightly hygroscopic mode is higher in the Aitken mode compared to the moderately hygroscopic mode in all seasons, except spring.

The separation of the two distinct hygroscopic modes, (a bimodal distribution or a continuum of mixing states), is most pronounced for the accumulation mode particles, (250 nm). The contribution of the moderately hygroscopic mode to the total hygroscopicity is higher compared to the hygroscopicity of Aitken particles. Particles larger than 100 nm are usually more aged than the smaller particles, with higher values of GF (Cubison et al., 2006), and more immediately associated with the atmospheric processing they undergo during long-range transport (Kalivitis et al., 2015). However, in winter time the expected slowing down of secondary aerosol formation processes and the existence of larger primary particles, partly from biomass burning (Bernardoni et al., 2017), make evident the distinct appearance of the fresh non and/or slightly hygroscopic mode and moderately hygroscopic mode in this size range. Moreover, looking at the GF-PDFs of the particles in the accumulation mode a peak appeared in the highly hygroscopic range. However, the number fraction corresponding to at peak is extremely so-low (i.e. close to zero). Thus, we decided that is unimportant to not to investigate further identify the truethe -nature of this negligible small-peak.

In order to investigate the hygroscopic properties of particles in more detailed, the temporal variability of mean GF, of standard deviation,  $\sigma$ , of individual GF-PDF measurements and of hygroscopicity parameter  $\kappa$ , was assessed by means of the box plots presented in fig. 5. for each month and for the dry diameteres, 30, 50, 80 and 250 nm.

The 30nm particles appeared to have a peak in GF during spring time, (April - May), and a second peak during late autumn-early winter, with a high variability in mean GF, (fig.5, Panel A). The 30 nm particles were internally mixed for all months with  $\sigma \leq 0.07$ , except from January and February, where the mean  $\sigma$  was 0.10 and 0.13, respectively (fig.5, Panel B). In the latter case the aerosol particles were externally mixed, (overlapping modes). Despite the fact that the monthly mean GF-PDFs in fig.S1 look similarly broad in February and April, the time-resolved data are quite different. In April the 30nm particles are characterized by low degree of mixing state, (always low sigma,  $\sigma = 0.07$ ), while considerable temporal variability in mean GF leads to a broad monthly mean GF-PDF. By contrast, in February, the mean GF exhibits limited variability, while the aerosol is externally mixed at any time ( $\sigma = 0.13$ ). The  $\kappa$  values corresponding to the mean GFs ranged from 0.11 to 0.33, (fig.5, Panel C).

The Aitken particles (50 nm and 80 nm) were characterized by a continuum of mixing states (externally mixed with overlapping modes), with  $\sigma$  values (fig.5, Panels E and H) ranging between 0.09 and 0.13, except from August, where the mean  $\sigma$  was 0.06, indicating an internally mixed aerosol. On average, the mean GFs and  $\kappa$  values of the Aitken particles appeared to follow the same trend as the 30 nm particles but with lower absolute values. The  $\kappa$  values of the Aitken particles, (fig.5, Panels F and I, respectively), ranged between 0.02 and 0.13.

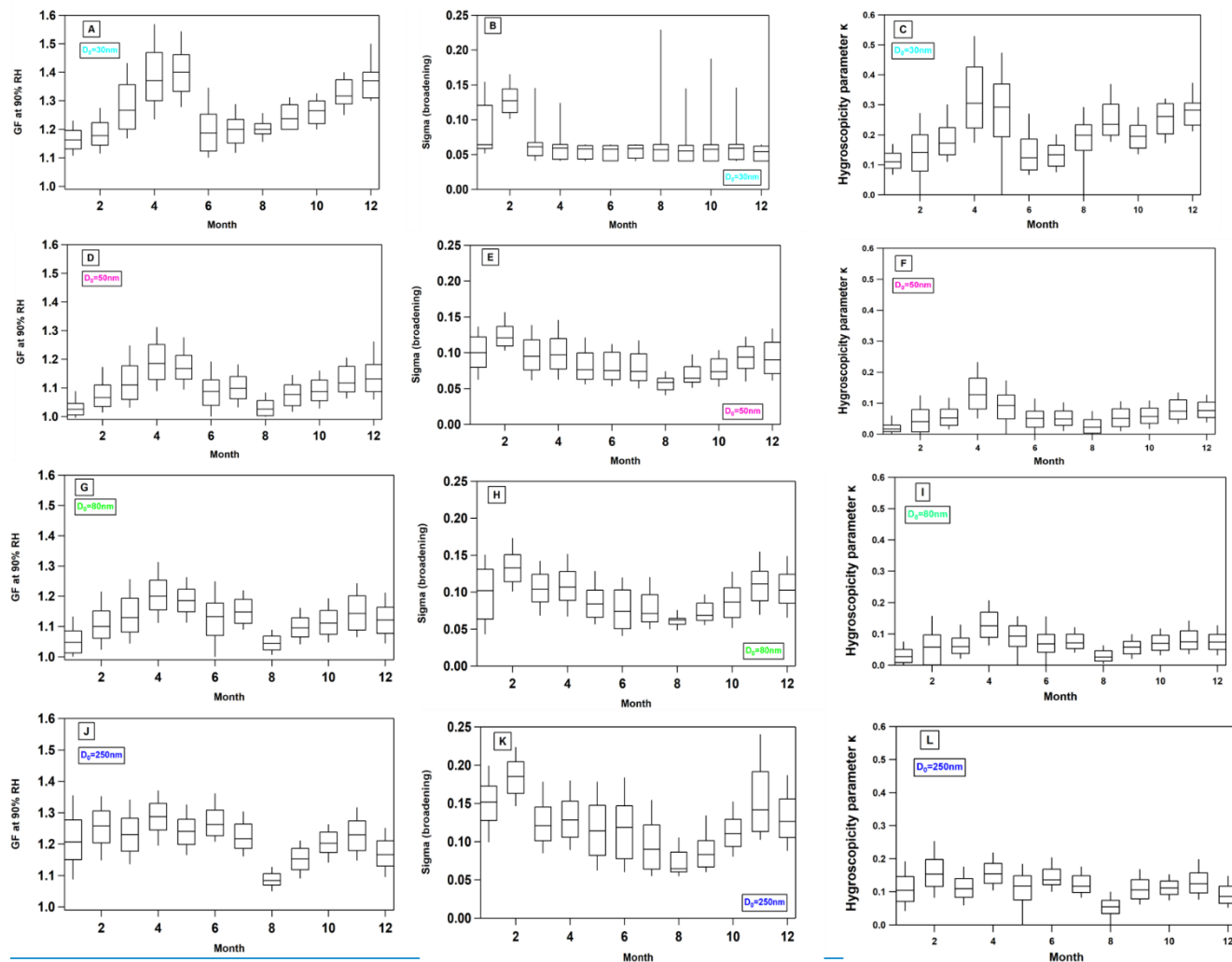
The  $D_0 = 250$  nm particles were characterized by a high degree of external mixing state, ( $0.09 \leq \sigma \leq 0.16$ , Panel K), during all months, except of August and September where the aerosol display a low degree of mixing state ( $\sigma = 0.09$ ). The mean GF and

$\kappa$  values were minimum in August (1.09, 0.03, respectively), and maximum in April (1.29, 0.13, respectively), indicating the seasonal variability in chemical composition of ambient aerosol throughout the year.

A higher degree of external mixing state in winter (February), was generally expected due to less effective aging process.

Exact magnitude and timing at this seasonal effect remains elusive based on a single year of observations.

285 The annual mean growth factors at 90 % relative humidity were found to be 1.28, 1.11, 1.13 and 1.22 for  $D_0 = 30, 50, 80$  and 250 nm, respectively. The mean values of hygroscopicity parameter  $\kappa$ , determined according to Equations (1) and (2), were found to be 0.22, 0.06, 0.08 and 0.12 for particles with dry diameters 30, 50, 80 and 250 nm, respectively.



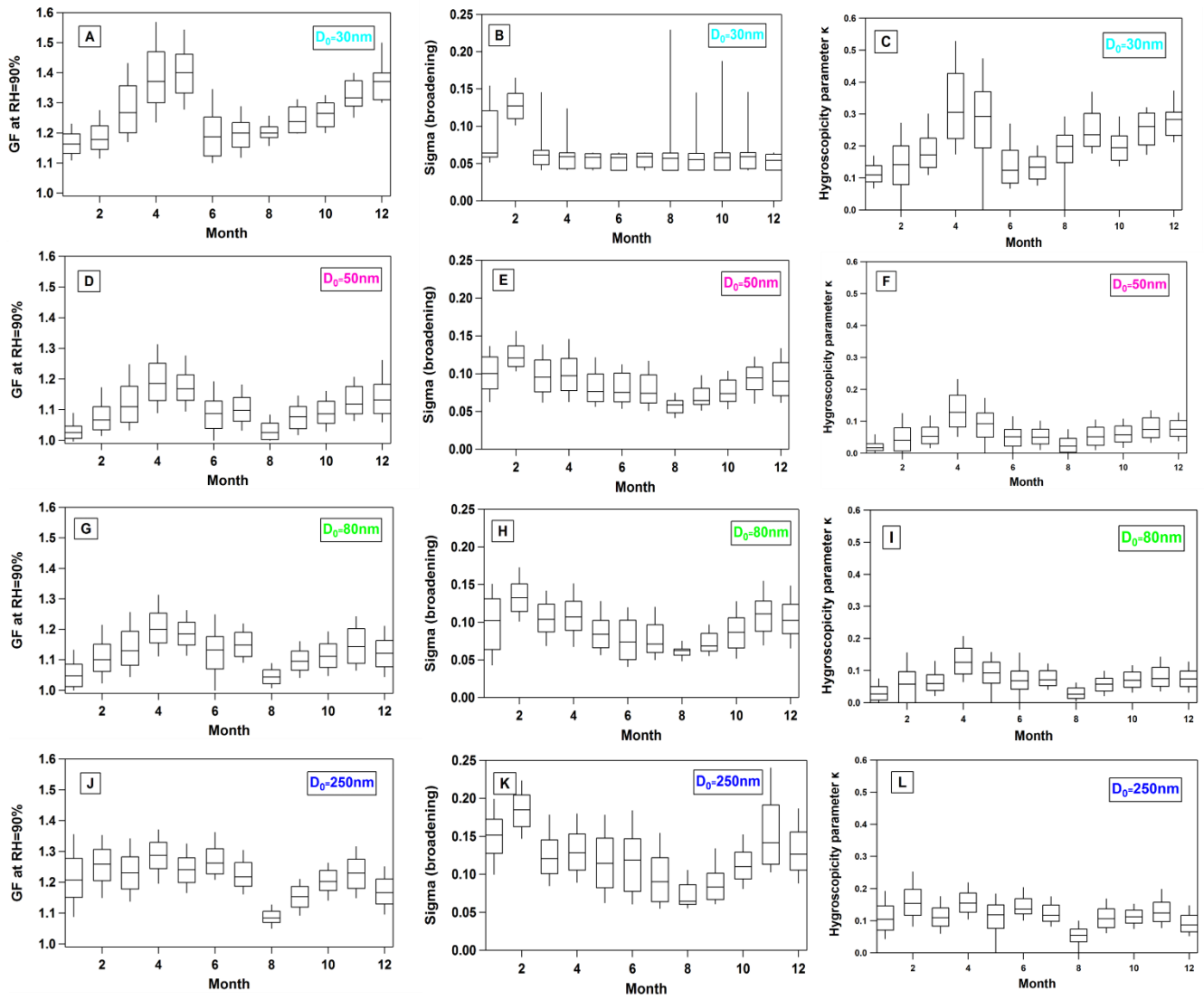
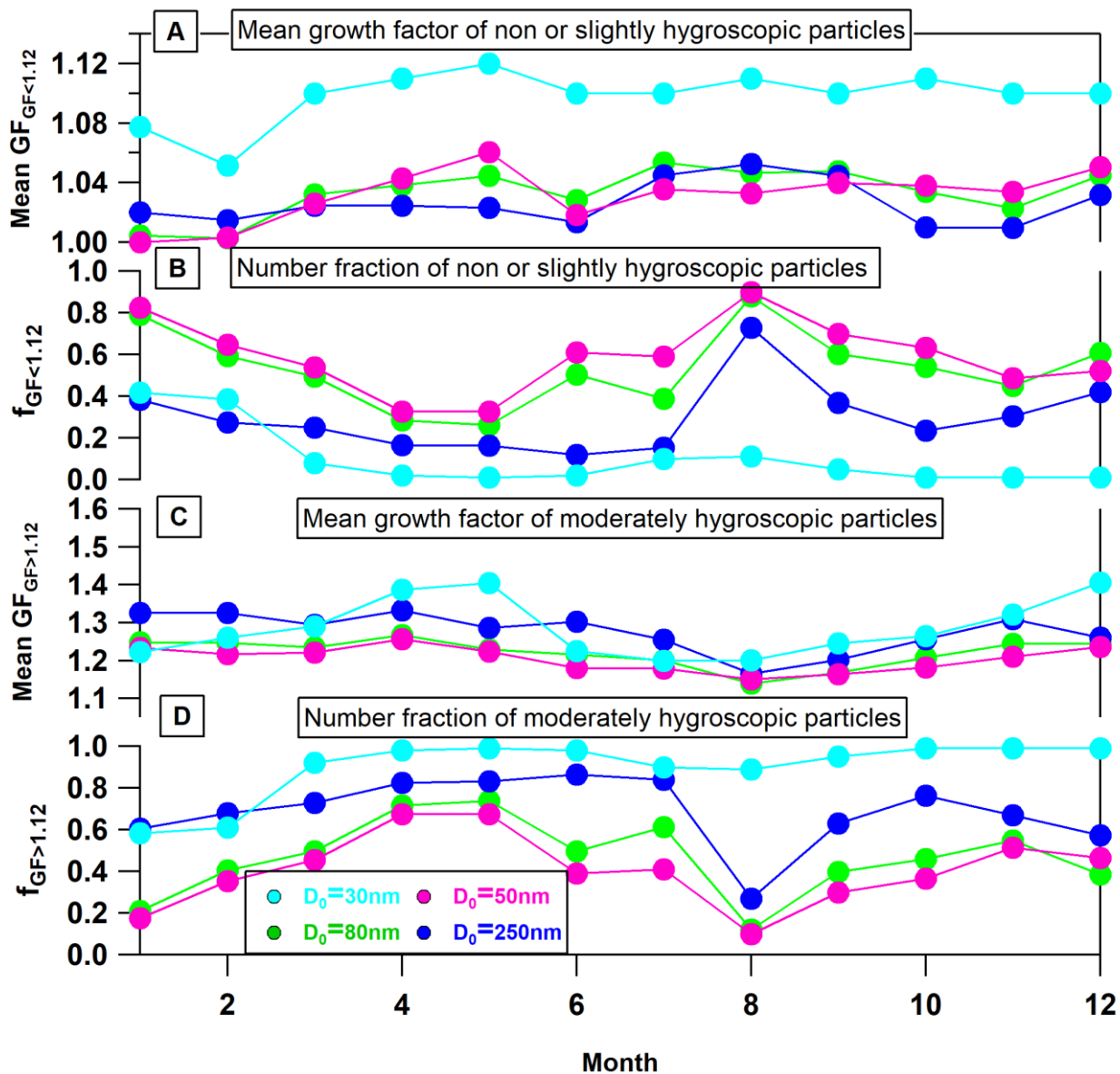


**Figure 5** Percentiles of the GF-PDF, standard deviation,  $\sigma$ , and hygroscopicity parameter  $\kappa$ , for each dry size and for each month. Box plots with whiskers show 10<sup>th</sup>, 25<sup>th</sup>, 50<sup>th</sup>, 75<sup>th</sup> and 90<sup>th</sup> percentiles.



295

**Figure 6** Annual cycles A) of the monthly mean GFs for non- or slightly hygroscopic particles at 90% RH, B) of number fraction of non- and/or slightly hygroscopic particles at 90% RH, C) of the monthly mean GFs for moderately hygroscopic particles at 90% RH, and D) of number fraction of moderately hygroscopic particles, for different particle sizes.

300 Figure 6 shows the monthly mean GFs and the number fraction,  $f_{GF}$ , of non and/or slightly hygroscopic and moderately hygroscopic mode, for each  $D_0$ . The variation of the mean GF for particles with  $GF < 1.12$  is expected to be relative low, given that the upper boundary of the non and/or slightly hygroscopic mode, (1.12), is quite low and close to the lowest boundary, (1.0). The mean GF of the moderately hygroscopic mode presented larger variability, with the minimum to be observed in

summer, (i.e. August). The mean GF of the subset with  $GF > 1.12$  was larger for the 30 nm and 250 nm particles compared with the 50 nm and 80 nm particles. The different hygroscopic properties of these particles reflect the differences in their chemical composition, with the particles in the nucleation and in the accumulation modes containing a larger fraction of more hygroscopic compounds, such as inorganics and more oxidized organics, compared to Aitken particles (Bougarioti et al., 2016). This trend in the size dependence of the mean GFs and consequently of the mean kappa values, is in line with the results from previous studies (Xu et al., 2019; Juranyi et al., 2013; Petäjä et al., 2007). Indicative GFs values for different chemical compounds are listed in Table 1.

The number fraction of each mode was also significantly different varied from month to month for all dry sizes, with distinct variability in the relative contributions of particles with small or moderate-to-large growth factors. For dry particle diameters  $D_0 > 30$  nm, the contribution of the non and/or slightly hygroscopic mode was minimum in spring and -maximum in August and in winter. For particles with  $D_0 = 250$  nm, the moderately hygroscopic particles clearly dominate over those with  $GF < 1.12$  for all seasons. Specifically, the number fraction of the moderately hygroscopic particles with  $D_0 = 250$  nm, were 0.62, 0.80, 0.67 and 0.70 in winter, spring, summer and autumn, respectively. This is consistent with the perception that the accumulation mode is dominated by aged aerosol (i.e. background aerosol), (Psichoudaki et al., 2018).

**TABLE 1** Mean Growth Factors measured at RH=90% for [particles with different chemical composition](#) old and warm period

Chemical Composition	Growth Factor, (GF)	Source
BC, Mineral Dust	<1.05	Vlasenko et al., 2005
Biomass Burning	1.15-1.65	Cocker et al., 2001
Aged wood smoke	1.3-1.5	Kotchenruther and Hobbs, 1998
Fresh wood smoke	1.1-1.3	Kotchenruther and Hobbs, 1998
Inorganic Ions	~1.7	Gysel et al., 2002
Organic Compounds	1.0-1.7	Koehler et al., 2006
<a href="#">Fresh traffic emission</a>	<a href="#">0.92-1.20</a>	<a href="#">Vu et al., 2021</a>
<a href="#">Aged traffic emission</a>	<a href="#">1.09-1.29</a>	<a href="#">Vu et al., 2021</a>

320

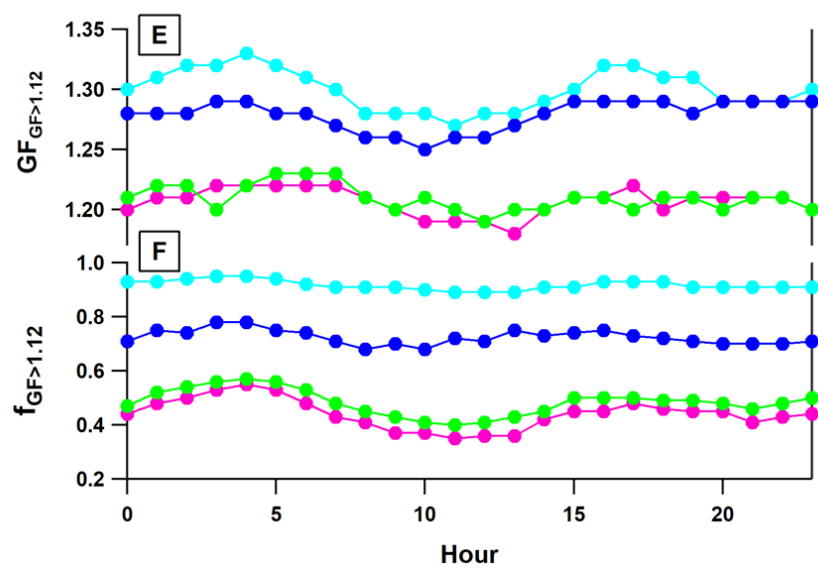
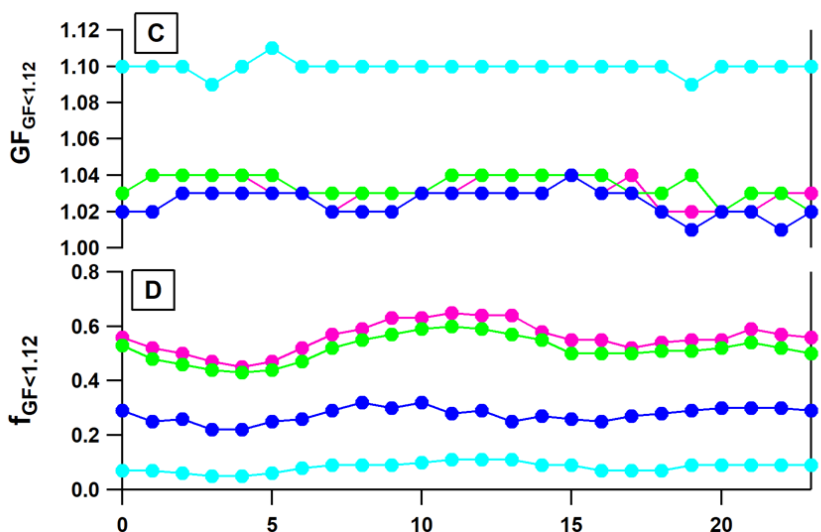
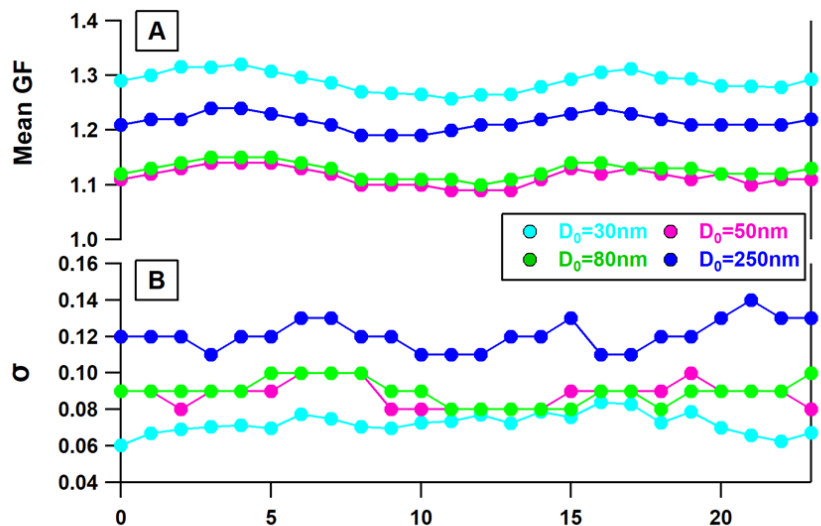
### 3.2 Annual and seasonal diurnal variability

The mean diurnal variability of critical meteorological parameters i.e. wind speed, temperature and relative humidity are shown in fig. S2. The daily average temperature varied between 17.2 °C and 20.5 °C, peaking at midday, whereas the average daily

325 relative humidity was ~ 60%, ranging between 68%, (night and early morning), and 49% (midday). The daily average wind speed varied between  $1.81 \text{ ms}^{-1}$  and  $2.84 \text{ ms}^{-1}$  peaking also at midday. Generally, higher concentrations of traffic-related pollutants are expected to be observed at the suburban site at midday, when conditions favour mixing and dispersion of the generated aerosol across the Athens valley. The prevailing westerly winds become stronger resulting in a well-mixed atmosphere, while the pollutants are transported from the city to the suburban site (Kalogridis et al., 2018). During the evening  
330 hours, a peak in the concentration levels of different air pollutant is typically observed reflecting the increased atmospheric stability (development of local inversion/nocturnal boundary layer), and emissions from different combustion sources especially in winter (i.e. residential heating), (Eleftheriadis et al., 2021).

Particle hygroscopicity was lower during morning rush hours, when an increase in the traffic-related emissions is expected to occur. In the afternoon an increase in hygroscopicity was observed which may be attributed to the condensation of water  
335 soluble organics and inorganics on fresh primary particles of local and regional origin (Psichoudaki et al., 2018). According to previous studies, the mass fraction of secondary organic compounds, which is generally higher in summer (Diapouli et al., 2017), peaks at noon, resulting in intermediate GF values ( $GF < 1.3$ ) a few hours later (Bourcier et al., 2012).

The diurnal mean GFs, standard deviation of mean GF,  $\sigma$ , and number fractions of the non and/or slightly hygroscopic and the moderately hygroscopic modes are presented in fig. 7, for each dry particle size. The Aitken particles are generally externally  
340 mixed throughout the day, with higher contribution of the moderately hygroscopic mode in the early morning (03:00-05:00). A second but less pronounced peak also appeared in the afternoon. The 24h cycle of the mean GF of the non and/or slightly hygroscopic mode ( $GF < 1.12$ ), appeared to have two peaks, with the major contribution of the non and/or slightly hygroscopic particles to occur at midday. Particles in the accumulation mode appeared to have a somewhat similar hygroscopic behaviour, in terms of diurnal variability, with Aitken particles, even though with less pronounced changes within the day for both growth  
345 factors and number fractions. [The standard deviations,  \$\sigma\$ , of subsets with  \$GF < 1.12\$  and  \$GF > 1.12\$  are presented in fig. S3.](#)



350 **Figure 7** Diurnal variation of A) mean GF, measured at RH=90% , B) standard deviation of the mean GF, C) GF of non or slightly hygroscopic particles, D) the number fraction of non or slightly hygroscopic particles, E) GF of moderately hygroscopic particles, and F) the number fraction of moderately hygroscopic particles

For the 30 nm particles, it was observed that the GF of the moderately hygroscopic mode was higher (GF > 1.3), between late evening and early morning (00:00 – 05:00 UTC+2), when the relative humidity appeared to have the maximum values (fig. S2) as well as at early afternoon (15:00 – 20:00 UTC+2), ~~whereas the minimum appeared at 21:00 UTC+2~~. At the DEM station, the 30 nm particles are ~~primarily generally~~ related to traffic emissions ~~and to a lesser extent to~~ ~~or~~ new particle formation (Vratolis, et al., 2019). This was also confirmed in the present study by the cluster analysis of the number size distributions. In fig.S34, the CPF (conditional probability function) ~~a~~ polar plot of 75<sup>th</sup> percentile of the total number concentration in the size range from 20 ~~nm~~ to 38 ~~nm~~ is presented (Carslaw and Ropkins, 2012). It is obvious that these particles are predominately originated from the urban area, under moderate wind speeds. Taking into account that the distance between Athens city center and DEM station is around 7 km, the transport time within the Athens value at the indicative wind speeds observed are yielding estimated transport time between ½ hour to a few hours. These data provide enough evidence to assume that the observed nuclei concentrations reflect a synergistic effect between different combustion-related urban emissions (e.g. fresh traffic-related aerosol from the neighborhood urban area and further growth) especially during daytime and the development of the local inversion boundary layer during night-time. As the particles undergo atmospheric aging their composition changes, in relative terms, ~~due to condensation of secondary aerosol. urban emission are the main source of these nuclei particles, while adequate time for further aging is also ensured. As the particles undergo atmospheric aging their composition changes, in relative terms, due to condensation of secondary aerosol which is most pronounced for the small particles.~~

360 During the photochemical active period of the day, the secondary formation of condensable organics, which might occur faster than that of inorganics, is probably responsible for the appearance of less hygroscopic Aitken particles (Mochida et al., 2008). Specifically, if the composition remains the same in the nuclei size range as for accumulation and Aitken mode particles, one would expect lower GFs for smaller particles (Kelvin effect). Here, it is evident that nuclei mode particles are more hygroscopic than the somewhat larger Aitken particles (Holmgren et al., 2014). This reflects the differences in the chemical composition between the nuclei mode and the lower end of Aitken particles, with the smaller particles to be a mixture of more hygroscopic compounds. Given that inorganics are more hygroscopic than organics, it is expected higher partitioning of the former to the nuclei size range, while the organics may be more crucial for further growth to larger particles.

370 During the photochemical active period of the day, (at noon), secondary formation of condensable organics, which might occur faster than that of inorganics, is probably responsible for the appearance of less hygroscopic Aitken particles than that of 30 nm, which is consistent with the findings presented in previous studies, (Mochida et al., 2008).

380 **3.3 Cluster analysis and aerosol hygroscopic properties**

Cluster analysis was performed on the hourly average size distributions in order to identify the link between aerosol hygroscopic properties, aerosol emission sources and particle formation mechanisms at the suburban area of Athens (fig. 8B). The mean GF-PDFs were calculated for each cluster and for the different dry particle sizes (fig. 8A). Differences in mean GF 385 between clusters were small, but trends in hygroscopicity across clusters were constituent for all particle sizes. Particle number size distributions vary across different regions and environments (Rose et al., 2021), and the structure of their patterns can be used as an indicator of the possible aerosol particle emission sources and formation processes. In DEM station, secondary aerosol formation, mostly related to sulphate and organics, and traffic-related emissions are the main sources of ambient aerosol, while biomass burning also consists a major source in winter (Vratolis et al., 2019; Bousiotis et al., 2021; Tsiflikiotou 390 et al., 2019; Kostenidou et al., 2015). In the present study, five clusters were identified which represent a combination of the major particle emission sources and formation/transformation processes. The modal characteristics of the clustered average number size distribution were summarized in Table S3.

395

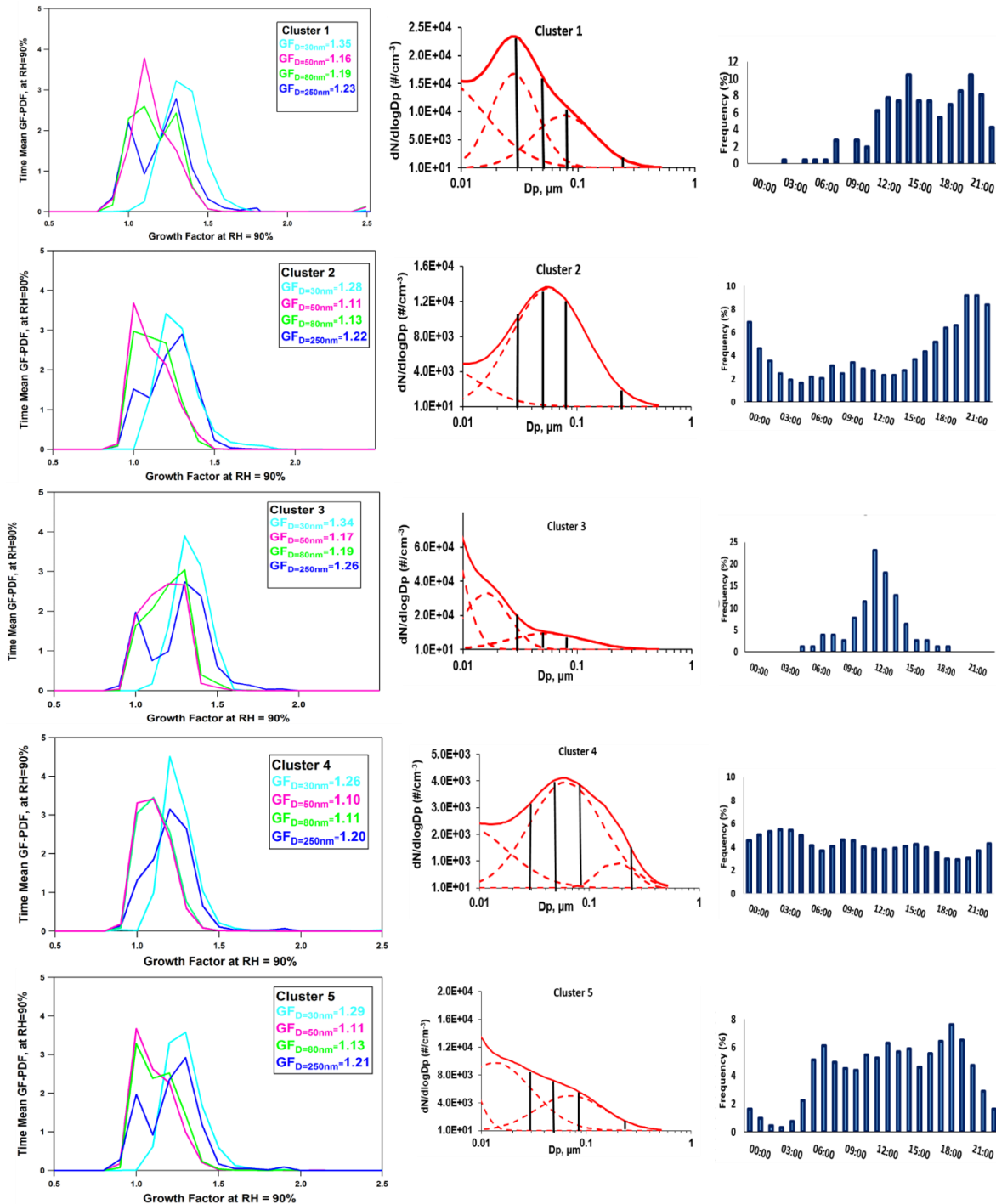


**Figure 8** A) Mean GF-PDF, B) Average number size distribution and C) Hourly frequency of occurrence for each cluster.

**Cluster 1 (Aged traffic mixed with background aerosol)** accounts for 4.2 % of the hourly particle number size distributions.

400 The fact that the frequency of the cluster occurrence peaks at noon and afternoon, while the morning traffic-related peak is missing, together with the prevailing westerly winds (fig. S45), hints to traffic-related pollution transported from the urban area.

**Cluster 2 (urban background, nocturnal)** represents 12.1% of the hourly averaged number size distributions. The diurnal frequency of occurrence profile of this cluster is characterized by an evening peak. The average particle number size 405 distribution has a major mode in the Aitken size range, which is probably a synergetic effect between particle emissions from different combustion sources (aged traffic, wood burning) and the development of the local inversion-nocturnal boundary layer.

**Cluster 3 (Nucleation and growth)** accounts for 1.3% of the hourly averaged number size distributions. The diurnal frequency of occurrence profile is characterized by a peak at noon and the nuclei mode at particle sizes < 10 nm seemed to contribute for 410 more than 60% to the total number concentration. This cluster was characterized by the least frequency of occurrence but the highest total number concentration, and occurs almost exclusively under westerly wind directions (fig. S45), of low to moderately wind speeds; conditions that favour new particle nucleation.

**Cluster 4 (Mixed urban and rUrban and regional background)** is the most frequent cluster (67%), dominated by aged and long-range transported aerosols and represents mainly the contribution of the regional/urban background aged aerosol, mostly 415 accounting for aged and long range transported aerosols. The diurnal profile is characterized by an almost stable frequency of occurrence within the day, and minimum total number concentrations (Brines et al., 2014). The major mode of the size distribution appeared in the Aitken size range (61 nm), while an additional mode also exists in the accumulation region.

**Cluster 5 (Traffic freshFresh traffic and further growth)** has a frequency of occurrence of 15.3% and is characterized by 420 a peak in the frequency of occurrence during morning and late afternoon traffic rush hours, -with an additional peak that appeared at noonwhile an additional peak appeared at noon. It is not restricted to a specific wind direction, while the size distribution is similar to cluster 1 but with higher contribution of nuclei particles to the total particle number concentration. This cluster represents the relatively fresh particles predominately transported in the receptor site from the neighbourhood urban area.

Specifically, clusters 2 and 5, which represent 12.1 % and 15.3% of the hourly averaged number size distributions, respectively 425 have similar GF-PDFs patterns and average GFs values for all dry particle sizes. Clusters 1 and 3, which account only for 4.2 % and 1.3 % of the hourly particle number size distributions and are related with atmospheric conditions favoring new particle formation or transport of nuclei particles from the city center to the sampling site, were characterized by more hygroscopic particles -(higher mean GFs) -compared to the other clusters. The particles of cluster 4, which represent 67% of the averaged 430 number size distributions, had the lowest mean GF values. The GF-PDF of the 30 nm appeared to have one moderately hygroscopic mode whose structure does not significantly between the clusters. For the larger particles, the distributions of the GFs appeared to have two modes with more or less distinct modes. In the case of cluster 4, which is mostly accounted for aged

and long-range transported particles, the GF-PDFs of the Aitken particles appeared to have a broad mode with no distinct modes, whereas the particles in the accumulation mode appeared to have two modes but less distinct than in the other clusters.

435

## Conclusions

The hygroscopic properties of ambient aerosol were investigated at a suburban environment in Athens, over a period of 12 months, using an HTDMA system for dry particles sizes of 30 nm, 50 nm, 80 nm and 250 nm at relative humidity<sub>5</sub> (RH), of 90%. The standard deviation  $\sigma$  of the inverted GF-PDF was used as a measure of the mixing state of aerosol. The aerosol was 440 characterized as internally, externally<sub>5</sub> (with two well-defined modes), or continuum of mixing states<sub>5</sub> (with two overlapping modes). In the case of an externally mixed aerosol, the growth factor spectrum was characterized by a non and/or slightly hygroscopic mode<sub>5</sub> (e.g. black carbon, fresh carbonaceous aerosol), and a moderately hygroscopic mode<sub>5</sub> (e.g. aged traffic, background aerosol).

The data were analyzed in term of their temporal seasonal and diurnal variability. The 30 nm particles were mostly internally 445 mixed and moderately hygroscopic in all seasons, except from wintertime, when a significant fraction of non and/or slightly hygroscopic mode became distinct. The 50 nm and 80 nm Aitken particles were mostly externally mixed except from August when an internally mixed and non and/or slightly hygroscopic aerosol type dominated this size fraction. The 250 nm particles were externally mixed, with the moderately hygroscopic mode being the major contributor to particle GFs<sub>5</sub> in all seasons. A 450 higher degree of external mixing state in winter (February)<sub>5</sub> was observed in all cases. This was generally expected due to the dominance of primary emissions from different combustion sources (i.e. biomass burning, traffic) and the less effective aging process under cold and dark conditions. Exact magnitude and timing at this seasonal effect remains elusive based on a single year of observations.

The number size distributions were also analyzed by means of cluster analysis to identify the link between aerosol 455 hygroscopicity and state of mixing and aerosol origin. The data were categorized into five clusters representative of traffic-related emission sources<sub>5</sub> (fresh and aged traffic), the mixed urban and regional background and urban-nocturnal aerosol and the photochemically induced new particle formation (nucleation). The clusters related with atmospheric conditions favouring new particle formation or transport of nuclei particles from the city centre, after undergoing further mixing with the background aerosol, are characterized by more hygroscopic nuclei particles compared to the other clusters. The mean GF-PDFs of the 460 Aitken particles and the particles in the accumulation size range revealed that their patterns are significantly associated with particle origin, being characterized by either a broad mode (urban and regional background aerosol), or two more or less distinct modes.

The HTDMA data obtained in this study can be further parameterized and used as a proxy for CCN prediction.

## **Data Availability**

465 Data are available upon request to the author ([spitieri@ipta.demokritos.gr](mailto:spitieri@ipta.demokritos.gr)).

## **Competing Interest**

The authors declare that they have no conflict of interest.

## **Author contributions**

470 CS performed the formal analysis and wrote the original draft. CS and MG performed the investigation and data curation. CS, MG and MGB provided the methodology and conceptualization. KE, MGB and MG provided supervision and validation. MG, KE, and MGB contributed to reviewing and editing the manuscript.

## **Acknowledgement**

475 This research is co-financed by Greece and the European Union (European Social Fund- ESF) through the Operational Programme «Human Resources Development, Education and Lifelong Learning» in the context of the project “Strengthening Human Resources Research Potential via Doctorate Research” (MIS-5000432), implemented by the State Scholarships Foundation (IKY).

480 We also acknowledge partial support by the project “PANhellenic infrastructure for Atmospheric Composition and climate change” (MIS 5021516), which is implemented under the Action “Reinforcement of the Research and Innovation Infrastructure”, funded by the Operational Program “Competitiveness, Entrepreneurship and Innovation” (NSRF 2014-2020) and co-financed by Greece and the European Union (European Regional Development Fund).

485 We also acknowledge partial support by the Action titled "National Network on Climate Change and its Impacts - CLIMPACT", funded by the Public Investment Program of Greece, General Secretariat of Research and Technology/Ministry of Development and Investments".

## **References**

Achttert, P., Birmili, W., Nowak, A., Wehner, B., Wiedensohler, A., Takegawa, N., Kondo, Y., Miyazaki, Y., Hu, M., and Zhu, T.: Hygroscopic growth of tropospheric particle number size distributions over the North China Plain, *J. Geophys. Res.*, 114, D00G07, doi:10.1029/2008JD010921, 2009.

Bernardoni, V., Elser, M., Valli, G., Valentini, S., Bigi, A., Fermo, P., Piazzalunga, A., Vecchi, R., Size-segregated aerosol in a hot-spot pollution urban area: Chemical composition and three-way source apportionment, (2017) *Environmental Pollution*, 231, pp. 601-61, 2017.

Bezantakos, S., Barmpounis, K., Giambarelu, M., Bossioli, E., Tombrou, M., Mihalopoulos, N., Eleftheriadis, K., Kalogiros, J., D. Allan, J., Bacak, A., Percival, C. J., Coe, H., and Biskos, G.: Chemical composition and hygroscopic properties of aerosol particles over the Aegean Sea, *Atmos. Chem. Phys.*, 13, 11595–11608, <https://doi.org/10.5194/acp-13-11595-2013>, 2013.

Bourcier, L., Sellegri, K., Chausse, P. et al. Seasonal variation of water-soluble inorganic components in aerosol size-segregated at the puy de Dôme station (1,465 m a.s.l.), France. *J Atmos Chem* 69, 47–66, <https://doi.org/10.1007/s10874-012-9229-2>, 2012.

Bougiatioti, A., Bezantakos, S., Stavroulas, I., Kalivitis, N., Kokkalis, P., Biskos, G., Mihalopoulos, N., Papayannis, A., and Nenes, A.: Biomass-burning impact on CCN number, hygroscopicity and cloud formation during summertime in the eastern Mediterranean, *Atmos. Chem. Phys.*, 16, 7389–7409, <https://doi.org/10.5194/acp-16-7389-2016>, 2016.

Bousiotis, D., Pope D., F., Beddows, C. S. D., Dall'Osto. M., Massling, A., Nøjgaard, K. J., Nordstrøm, C., Niemi, V. J., Portin, H., Petäjä, T., Perez, N., Alastuey, A., Querol, X., Kouvarakis, G., Mihalopoulos, N., Vratolis, S., Eleftheriadis, K., Wiedensohler, A., Weinhold, K., Merkel, M., Tuch, T., and Harrison M. R., *Atmos. Chem. Phys.*, 21, 11905–11925, <https://doi.org/10.5194/acp-21-11905-2021>, 2021

Brines, M. Dall’Osto, M., Beddows, D.C.S., Harrison, R. M., and Querol, X., Simplifying aerosol size distributions modes simultaneously detected at four monitoring sites during SAPUSS. *Atmos. Chem. Phys.*, 14, 2973–2986, 2014.

Cubison, M. J., Alfarra, M. R., Allan, J., Bower, K. N., Coe, H., McFiggans, G. B., Whitehead, J. D., Williams, P. I., Zhang, Q., Jimenez, J. L., Hopkins, J., and Lee, J.: The characterization of pollution aerosol in a changing photochemical environment, *Atmos. Chem. Phys.*, 6, 5573–5588, <https://doi.org/10.5194/acp-6-5573-2006>, 2006.

Carslaw, D. C. and Ropkins, K.: openair –An R package for air quality data analysis, *Environ. Model. Softw.*, 27–28, 52–61, <https://doi.org/10.1016/j.envsoft.2011.09.008>, 2012

Dean A. Hegg, David S. Covert, Haflidi Jonsson, Paul A. Covert.: An Instrument for Measuring Size-Resolved Aerosol Hygroscopicity at both Sub- and Super-Micron Sizes, *Aerosol Science and Technology*, 41:9, 873-883, DOI: 10.1080/02786820701506955, 2007.

David R. Cocker III, Nathan E. Whitlock, Richard C. Flagan & John H. Seinfeld.: Hygroscopic Properties of Pasadena, California Aerosol, *Aerosol Science and Technology*, 35:2, 637-647, DOI: 10.1080/02786820120653, 2001.

Diapouli, E.; Kalogridis, A.-C.; Markantonaki, C.; Vratolis, S.; Fefatidis, P.; Colombi, C.; Eleftheriadis, K. Annual Variability of Black Carbon Concentrations Originating from Biomass and Fossil Fuel Combustion for the Suburban Aerosol in Athens, Greece. *Atmosphere* 2017, 8, 234. <https://doi.org/10.3390/atmos8120234>, 2017.

Eleftheriadis, K., Gini, M.I., Diapouli, Vratolis S., Vasilatou V., Fefatidis P., Manousakkas I. M.: Aerosol microphysics and chemistry reveal the COVID19 lockdown impact on urban air quality. *Scientific Reports* 11, 14477, <https://doi.org/10.1038/s41598-021-93650-6>, 2021.

Enroth, J., Mikkilä, J., Németh, Z., Kulmala, M., and Salma, I.: Wintertime hygroscopicity and volatility of ambient urban aerosol particles, *Atmos. Chem. Phys.*, 18, 4533–4548, <https://doi.org/10.5194/acp-18-4533-2018>, 2018.

Fors, E. O., Swietlicki, E., Svenningsson, B., Kristensson, A., Frank, G. P., and Sporre, M.: Hygroscopic properties of the ambient aerosol in southern Sweden – a two year study, *Atmos. Chem. Phys.*, 11, 8343–8361, <https://doi.org/10.5194/acp-11-8343-2011>, 2011.

530 Gunthe, S. S., King, S. M., Rose, D., Chen, Q., Roldin, P., Farmer, D. K., Jimenez, J. L., Artaxo, P., Andreae, M. O., Martin, S. T., and Pöschl, U.: Cloud condensation nuclei in pristine tropical rainforest air of Amazonia: size-resolved measurements and modeling of atmospheric aerosol composition and CCN activity, *Atmos. Chem. Phys.*, 9, 7551–7575, <https://doi.org/10.5194/acp-9-7551-2009>, 2009.

Gysel, M., Crosier, J., Topping, D. O., Whitehead, J. D., Bower, K. N., Cubison, M. J., Williams, P. I., Flynn, M. J., McFiggans, G. B., and Coe, H.: Closure study between chemical composition and hygroscopic growth of aerosol particles during TORCH2, *Atmos. Chem. Phys.*, 7, 6131–6144, <https://doi.org/10.5194/acp-7-6131-2007>, 2007.

535 Gysel, M., McFiggans, G.B., Coe, H., Inversion of tandem differential mobility analyser (TDMA) measurements, *Journal of Aerosol Science*, Volume 40, Issue 2, 134-151, ISSN 0021-8502, <https://doi.org/10.1016/j.jaerosci.2008.07.013>, 2009.

Gysel M, Weingartner E, Baltensperger U. Hygroscopicity of aerosol particles at low temperatures. 2. Theoretical and 540 experimental hygroscopic properties of laboratory generated aerosols. *Environ Sci Technol*. 2002 Jan 1;36(1):63-8. doi: 10.1021/es010055g. PMID: 11811491, 2002.

Haywood, J., and Boucher, O.: Estimates of the direct and indirect radiative forcing due to tropospheric aerosols: A review, *Rev. Geophys.*, 38( 4), 513– 543, doi:10.1029/1999RG000078, 2000.

Hussein T., Mølgaard, B., Hannuniemi, H., Martikainen, J., Järvi, L., Wegner, T., Ripamonti, G., Weber, S., Vesala, T. & 545 Hämeri, K.: Fingerprints of the urban particle number size distribution in helsinki, Finland: local versus regional characteristics. *Boreal Env. Res.* 19: 1–20, 2014.

Hussein T., Hämeri K., Aalto P., Paatero P., Kulmala M., Modal structure and spatial–temporal variations of urban and suburban aerosols in Helsinki—Finland, *Atmospheric Environment*, Volume 39, Issue 9, Pages 1655-1668, ISSN 1352-2310, <https://doi.org/10.1016/j.atmosenv.2004.11.031>, 2005.

550 Holmgren, H., Sellegrí, K., Hervo, M., Rose, C., Freney, E., Villani, P., and Laj, P.: Hygroscopic properties and mixing state of aerosol measured at the high-altitude site Puy de Dôme (1465 m a.s.l.), France, *Atmos. Chem. Phys.*, 14, 9537–9554, <https://doi.org/10.5194/acp-14-9537-2014>, 2014.

IPCC: Climate Change 2013: The Physical Science Basis. Contribution of Working Group I to the Fifth Assessment Report of the Intergovernmental Panel on Climate Change, Cambridge University Press, Cambridge, UK and Neew York, NY, USA, 555 2013.

Jurányi, Z., Tritscher, T., Gysel, M., Laborde, M., Gomes, L., Roberts, G., Baltensperger, U., and Weingartner, E.: Hygroscopic mixing state of urban aerosol derived from size-resolved cloud condensation nuclei measurements during the MEGAPOLI campaign in Paris, *Atmos. Chem. Phys.*, 13, 6431–6446, <https://doi.org/10.5194/acp-13-6431-2013>, 2013.

560 Kammermann, L., Gysel, M., Weingartner, E., and Baltensperger, U.: 13-month climatology of the aerosol hygroscopicity at the free tropospheric site Jungfraujoch (3580 m a.s.l.), *Atmos. Chem. Phys.*, 10, 10717–10732, <https://doi.org/10.5194/acp-10-10717-2010>, 2010.

Kanakidou, M., Seinfeld, J. H., Pandis, S. N., Barnes, I., Dentener, F. J., Facchini, M. C., Van Dingenen, R., Ervens, B., Nenes, A., Nielsen, C. J., Swietlicki, E., Putaud, J. P., Balkanski, Y., Fuzzi, S., Horth, J., Moortgat, G. K., Winterhalter, R., Myhre, C. E. L., Tsigaridis, K., Vignati, E., Stephanou, E. G., and Wilson, J.: Organic aerosol and global climate modelling: a review, *Atmos. Chem. Phys.*, 5, 1053–1123, <https://doi.org/10.5194/acp-5-1053-2005>, 2005.

Kalivitis, N., Kerminen, V.-M., Kouvarakis, G., Stavroulas, I., Bougiatioti, A., Nenes, A., Manninen, H. E., Petäjä, T., Kulmala, M., and Mihalopoulos, N.: Atmospheric new particle formation as a source of CCN in the eastern Mediterranean marine boundary layer, *Atmos. Chem. Phys.*, 15, 9203–9215, <https://doi.org/10.5194/acp-15-9203-2015>, 2015.

Kaufman, Y., Tanré, D. & Boucher, O. A satellite view of aerosols in the climate system. *Nature* 419, 215–223, <https://doi.org/10.1038/nature01091>, 2002.

Kalogridis, A. C., Vratolis, S., Liakakou, E., Gerasopoulos, E., Mihalopoulos, N., and Eleftheriadis, K., Assessment of wood burning versus fossil fuel contribution to wintertime black carbon and carbon monoxide concentrations in Athens, Greece, *Atmos. Chem. Phys.*, 18, 10219–10236, 2018, <https://doi.org/10.5194/acp-18-10219-2018>

Kim, N., Yum, S. S., Park, M., Park, J. S., Shin, H. J., and Ahn, J. Y.: Hygroscopicity of urban aerosols and its link to size-resolved chemical composition during spring and summer in Seoul, Korea, *Atmos. Chem. Phys.*, 20, 11245–11262, <https://doi.org/10.5194/acp-20-11245-2020>, 2020.

Koehler, K. A., Kreidenweis, S. M., DeMott, P. J., Prenni, A. J., Carrico, C. M., Ervens, B., and Feingold, G.: Water activity and activation diameters from hygroscopicity data - Part II: Application to organic species, *Atmos. Chem. Phys.*, 6, 795–809, <https://doi.org/10.5194/acp-6-795-2006>, 2006.

580 Köhler, H.: The nucleous in the growth of hygroscopic droplets, *Trans. Faraday Soc.*, 32, 1152–1161, 1936.

Kostenidou, E., Florou, K., Kaltsonoudis, C., Tsiflikiotou, M., Vratolis, S., Eleftheriadis, K., and Pandis, S. N.: Sources and chemical characterization of organic aerosol during the summer in the eastern Mediterranean, *Atmos. Chem. Phys.*, 15, 11355–11371, <https://doi.org/10.5194/acp-15-11355-2015>, 2015.

Kotchenruther, R. A. & Hobbs, P. V. Humidification factors of aerosols from biomass burning in Brazil. *J. Geophys. Res. Atmospheres* 103, 32081–32089, 1998.

[Petters, M. D., and S. M. Kreidenweis \(2007\). A single parameter representation of hygroscopic growth and cloud condensation nucleus activity, \*Atmos. Chem. Phys.\*, 7\(8\), 1961–1971, 2007.](#)

Z. L. Li, W. K.-M.Ramanathan, V.Wu, G.Ding, Y.Manoj, M. G.Liu, J.Qian, Y.Li, J.Zhou, T.Fan, J.Rosenfeld, D.Ming, Y.Wang, Y.Huang, J.Wang, B.Xu, X.Lee, S.-S.Cribb, M.Zhang, F.Yang, X.Zhao, C.Takemura, T.Wang, K.Xia, X.Yin, 590 Y.Zhang, H.Guo, J.Zhai, P. M.Sugimoto, N.Babu, S. S.Brasseur, G. P.:Aerosol and monsoon climate interactions over Asia, *Rev. Geophys.*, 54, 866– 929, doi:10.1002/2015RG000500, 2016.

McFiggans, G., Artaxo, P., Baltensperger, U., Coe, H., Facchini, M. C., Feingold, G., Fuzzi, S., Gysel, M., Laaksonen, A., Lohmann, U., Mentel, T. F., Murphy, D. M., O'Dowd, C. D., Snider, J. R., and Weingartner, E.: The effect of physical and chemical aerosol properties on warm cloud droplet activation, *Atmos. Chem. Phys.*, 6, 2593–2649, <https://doi.org/10.5194/acp-6-2593-2006>, 2006.

595 Massling, A., Leinert, S., Wiedensohler, A., and Covert, D.: Hygroscopic growth of sub-micrometer and one-micrometer aerosol particles measured during ACE-Asia, *Atmos. Chem. Phys.*, 7, 3249–3259, <https://doi.org/10.5194/acp-7-3249-2007>, 2007.

600 Mochida, Michihiro & Miyakawa, Takuma & Takegawa, Nobuyuki & Morino, Yu & Kawamura, Kimitaka & Kondo, Yutaka.: Significant alteration in the hygroscopic properties of urban aerosol particles by the secondary formation of organics. *Geophys. Res. Lett.* 35. 10.1029/2007GL031310, 2008.

Motos, G., Schmale, J., Corbin, J. C., Zanatta, M., Baltensperger, U., and Gysel-Beer, M.: Droplet activation behaviour of atmospheric black carbon particles in fog as a function of their size and mixing state. *Atmos. Chem. Phys.*, 19, 2183-2207, doi:10.5194/acp-19-2183-2019, 2019.

605 Paramonov, M., Kerminen, V.-M., Gysel, M., Aalto, P. P., Andreae, M. O., Asmi, E., Baltensperger, U., Bougiatioti, A., Brus, D., Frank, G. P., Good, N., Gunthe, S. S., Hao, L., Irwin, M., Jaatinen, A., Jurányi, Z., King, S. M., Kortelainen, A., Kristensson, A., Lihavainen, H., Kulmala, M., Lohmann, U., Martin, S. T., McFiggans, G., Mihalopoulos, N., Nenes, A., O'Dowd, C. D., Ovadnevaite, J., Petäjä, T., Pöschl, U., Roberts, G. C., Rose, D., Svenningsson, B., Swietlicki, E., Weingartner, E., Whitehead, J., Wiedensohler, A., Wittbom, C., and Sierau, B.: A synthesis of cloud condensation nuclei counter (CCNC) measurements within the EUCAARI network, *Atmos. Chem. Phys.*, 15, 12211–12229, <https://doi.org/10.5194/acp-15-12211-2015>, 2015.

610 Psichoudaki M., Nenes A., Florou K., Kaltsoudis C., Pandis N.S.: Hygroscopic properties of atmospheric particles emitted during wintertime biomass burning episodes in Athens, *Atmospheric Environment*, Volume 178, 2018, Pages 66-72, ISSN 1352-2310, <https://doi.org/10.1016/j.atmosenv.2018.01.004>, 2018.

615 Petters, M. D., and S. M. Kreidenweis (2007), A single parameter representation of hygroscopic growth and cloud condensation nucleus activity, *Atmos. Chem. Phys.*, 7(8), 1961–1971, 2007.

Petters, M. D. AND Kreidenweis, S.M.: A single parameter representation of hygroscopic growth and cloud condensation nucleus activity, *Atmos. Chem. Phys.*, 7, 1961-1971, doi:10.5194/acp-7-1961-2007, 2007.

Petäjä, T., Kerminen, V.-M., Dal Maso, M., Junninen, H., Koponen, I. K., Hussein, T., Aalto, P. P., Andronopoulos, S., Robin, 620 D., Hämeri, K., Bartzis, J. G., and Kulmala, M.: Sub-micron atmospheric aerosols in the surroundings of Marseille and Athens: physical characterization and new particle formation, *Atmos. Chem. Phys.*, 7, 2705–2720, <https://doi.org/10.5194/acp-7-2705-2007>, 2007.

Rose, C., Collaud Coen, M., Andrews, E., Lin, Y., Bossert, I., Lund Myhre, C., Tuch, T., Wiedensohler, A., Fiebig, M., Aalto, P., Alastuey, A., Alonso-Blanco, E., Andrade, M., Artíñano, B., Arsov, T., Baltensperger, U., Bastian, S., Bath, O., Beukes, J. 625 P., Brem, B. T., Bukowiecki, N., Casquero-Vera, J. A., Conil, S., Eleftheriadis, K., Favez, O., Flentje, H., Gini, M. I., Gómez-

Moreno, F. J., Gysel-Bear, M., Hallar, A. G., Kalapov, I., Kalivitis, N., Kasper-Giebl, A., Keywood, M., Kim, J. E., Kim, S.-W., Kristensson, A., Kulmala, M., Lihavainen, H., Lin, N.-H., Lyamani, H., Marinoni, A., Martins Dos Santos, S., Mayol-Bracero, O. L., Meinhardt, F., Merkel, M., Metzger, J.-M., Mihalopoulos, N., Ondracek, J., Pandolfi, M., Pérez, N., Petäjä, T., Petit, J.-E., Picard, D., Pichon, J.-M., Pont, V., Putaud, J.-P., Reisen, F., Sellegri, K., Sharma, S., Schauer, G., Sheridan, P.,  
630 Sherman, J. P., Schwerin, A., Sohmer, R., Sorribas, M., Sun, J., Tulet, P., Vakkari, V., van Zyl, P. G., Velarde, F., Villani, P., Vratolis, S., Wagner, Z., Wang, S.-H., Weinhold, K., Weller, R., Yela, M., Zdimal, V., and Laj, P.: Seasonality of the particle number concentration and size distribution: a global analysis retrieved from the network of Global Atmosphere Watch (GAW) near-surface observatories, *Atmos. Chem. Phys.*, 21, 17185–17223, <https://doi.org/10.5194/acp-21-17185-2021>, 2021.

Riemer, N., Ault, A. P., West, M., Craig, R. L., & Curtis, J. H.: Aerosol mixing state: Measurements, modeling, and impacts.  
635 *Reviews of Geophysics*, 57, 187–249. <https://doi.org/10.1029/2018RG000615>, 2019.

Rosenfeld, D., Andreae, M. O., Asmi, A., Chin, M., Leeuw, G., Donovan, D. P., Kahn, R., Kinne, S., Kivekäs, N., Kulmala, M., Lau, W., Schmidt, K. S., Suni, T., Wagner, T., Wild, M., Quaas, J.: Global observations of aerosol-cloud-precipitation-climate interactions, *Rev. Geophys.*, 52, 750–808, doi:10.1002/2013RG000441, 2014.

Sjogren, S., Gysel, M., Weingartner, E., Alfarra, M. R., Duplissy, J., Cozic, J., Crosier, J., Coe, H., and Baltensperger, U.:  
640 Hygroscopicity of the submicrometer aerosol at the high-alpine site Jungfraujoch, 3580 m a.s.l., Switzerland, *Atmos. Chem. Phys.*, 8, 5715–5729, <https://doi.org/10.5194/acp-8-5715-2008>, 2008.

Tsiflikiotou, M.A., Kostenidou, E., Papanastasiou, D.K., Patoulas, D., Zarmpas, P., Paraskevopoulou, D., Diapouli, E., Kaltonoudis, C., Florou, K., Bougiatioti, A., Stavroulas, I., Theodosi, C., Kouvarakis, G., Vasilatou, V., Siakavaras, D., Biskos, G., Pilinis, C., Eleftheriadis, K., Gerasopoulos, E., Mihalopoulos, N., Pandis, S.N. (2019) Summertime particulate matter and  
645 its composition in Greece. *Atmospheric Environment*, 213. 597-607 doi:10.1016/j.atmosenv.2019.06.013, 2019.

Schmale, J., Henning, S., Henzing, B., Gysel, M.: Collocated observations of cloud condensation nuclei, particle size distributions, and chemical composition. *Sci. Data* 4,170003, doi: 10.1038/sdata.2017.3, 2017.

Schmale, J., Henning, S., Decesari, S., Henzing, B., Keskinen, H., Sellegri, K., Ovadnevaite, J., Pöhlker, M. L., Brito, J., Bougiatioti, A., Kristensson, A., Kalivitis, N., Stavroulas, I., Carbone, S., Jefferson, A., Park, M., Schlag, P., Iwamoto, Y., Aalto, P., Äijälä, M., Bukowiecki, N., Ehn, M., Frank, G., Fröhlich, R., Frumau, A., Herrmann, E., Herrmann, H., Holzinger, R., Kos, G., Kulmala, M., Mihalopoulos, N., Nenes, A., O'Dowd, C., Petäjä, T., Picard, D., Pöhlker, C., Pöschl, U., Poulain, L., Prévôt, A. S. H., Swietlicki, E., Andreae, M. O., Artaxo, P., Wiedensohler, A., Ogren, J., Matsuki, A., Yum, S. S., Stratmann, F., Baltensperger, U., and Gysel, M.: Long-term cloud condensation nuclei number concentration, particle number size distribution and chemical composition measurements at regionally representative observatories, *Atmos. Chem. Phys.*, 18, 2853–2881,  
650 https://doi.org/10.5194/acp-18-2853-2018, 2018.

Swietlicki, E., Hansson, H-C., Hameri, K., Svenningsson, B., Massling, A., McFiggans, G., McMurry, P. H., Petäjä, T., Tunved, P., Gysel, M., Topping, D., Weingartner, E., Baltensperger, U., Rissler, J., Wiedensohler, A., & Kulmala, M.: Hygroscopic properties of submicrometer atmospheric aerosol particles measured with H-TDMA instruments in various environments - a  
655

review. *Tellus. Series B: Chemical and Physical Meteorology*, 60(3), 432-469. <https://doi.org/10.1111/j.1600-0889.2008.00350.x>, 2008.

660 Tritscher, T., Dommen, J., DeCarlo, P. F., Gysel, M., Barmet, P. B., Praplan, A. P., Weingartner, E., Prévôt, A. S. H., Riipinen, I., Donahue, N. M., and Baltensperger, U.: Volatility and hygroscopicity of aging secondary organic aerosol in a smog chamber, *Atmos. Chem. Phys.*, 11, 11477–11496, <https://doi.org/10.5194/acp-11-11477-2011>, 2011.

665 Vratolis S., Gini M. I., Bezentakos S., Stavroulas I., Kalivitis N., Kostenidou E., Louvaris E., Siakavaras D. Biskos G., Mihalopoulos N., Pandis S. N., Pilinis C., Papayannis A., and Eleftheriadis K.: Particle number size distribution statistics at city-centre, urban background, and remote stations in Greece during summer, *Atmos. Environ.*, 213, 711-726, 2019.

Vu, T.V., Shi, Z. & Harrison, R.M. Estimation of hygroscopic growth properties of source-related sub-micrometre particle types in a mixed urban aerosol, *Clim. Atmos. Sci.* 4, 21, <https://doi.org/10.1038/s41612-021-00175-w>, 2021.

670 Vlasenko, S. Sjögren, E. Weingartner, H. W. Gäggeler & M. Ammann.: Generation of Submicron Arizona Test Dust Aerosol: Chemical and Hygroscopic Properties, *Aerosol Science and Technology*, [39:5,452-460](https://doi.org/10.1080/027868290959870), DOI: 10.1080/027868290959870, 2005.

675 Wang, X., Shen, X. J., Sun, J.Y., Zhang, X.Y., Wang, Y.Q., Zhang, Y. M., Wang, P., Xia, C., Qi, X. F., Zhong, J. T.: Size-resolved hygroscopic behavior of atmospheric aerosols during heavy aerosol pollution episodes in Beijing in December 2016, *Atmospheric Environment*, Volume 194, 2018, Pages 188-197, ISSN 1352-2310, <https://doi.org/10.1016/j.atmosenv.2018.09.041>, 2018.

680 Wiedensohler, A., Birmili, W., Nowak, A., Sonntag, A., Weinhold, K., Merkel, M., Wehner, B., Tuch, T., Pfeifer, S., Fiebig, M., Fjäraa, A. M., Asmi, E., Sellegrí, K., Depuy, R., Venzac, H., Villani, P., Laj, P., Aalto, P., Ogren, J. A., Swietlicki, E., Williams, P., Roldin, P., Quincey, P., Hüglin, C., Fierz-Schmidhauser, R., Gysel, M., Weingartner, E., Riccobono, F., Santos, S., Grüning, C., Falloon, K., Beddows, D., Harrison, R., Monahan, C., Jennings, S. G., O'Dowd, C. D., Marinoni, A., Horn, H.-G., Keck, L., Jiang, J., Scheckman, J., McMurry, P. H., Deng, Z., Zhao, C. S., Moerman, M., Henzing, B., de Leeuw, G., Löschau, G., and Bastian, S.: Mobility particle size spectrometers: harmonization of technical standards and data structure to facilitate high quality long-term observations of atmospheric particle number size distributions, *Atmos. Meas. Tech.*, 5, 657–685, <https://doi.org/10.5194/amt-5-657-2012>, 2012.

685 Xu, W., Sun, Y., Wang, Q., Zhao, J., Wang, J., Ge, X., Xie, C., Zhou, W., Du, W., Li, J., Fu, P., Wang, Z., Worsnop, R. D., Coe, H.: Changes in aerosol chemistry from 2014 to 2016 in winter in Beijing: Insights from high-resolution aerosol mass spectrometry. *Journal of Geophysical Research: Atmospheres*, 124, 1132– 1147. <https://doi.org/10.1029/2018JD029245>, 2019.

Zhang, Q., Jimenez, J. L., Canagaratna, M. R., Ulbrich, I. M., Ng, N. L., Worsnop, D. R., Sun, Y.,: Understanding atmospheric organic aerosols via factor analysis of aerosol mass spectrometry: a review. *Anal BioanalChem*401, 3045–3067, <https://doi.org/10.1007/s00216-011-5355-y>, 2011.

690